Update of short-baseline electron neutrino and antineutrino disappearance

C. Giunti
INFN, Sezione di Torino, Via P. Giuria 1, I-10125 Torino, Italy

M. Laveder
Dipartimento di Fisica e Astronomia "G. Galilei", Università di Padova and INFN, Sezione di Padova, Via F. Marzolo 8, I-35131 Padova, Italy

Y. F. Li
Institute of High Energy Physics, Chinese Academy of Sciences, Beijing 100049, China

Q. Y. Liu and H. W. Long
Department of Modern Physics, University of Science and Technology of China, Hefei, Anhui 230026, China
(Received 30 October 2012; published 26 December 2012)

We present a complete update of the analysis of ν_e and $\bar{\nu}_e$ disappearance experiments in terms of neutrino oscillations in the framework of 3 + 1 neutrino mixing, taking into account the Gallium anomaly, the reactor anomaly, solar neutrino data, and ν_eC scattering data. We discuss the implications of a recent ^{71}Ga(^{3}He, ^{3}H)^{71}Ge measurement which give information on the neutrino cross section in Gallium experiments. We discuss the solar bound on active-sterile mixing and present our numerical results. We discuss the connection between the results of the fit of neutrino oscillation data and the heavy neutrino mass effects in β-decay experiments (considering new Mainz data) and neutrinoless double-β decay experiments (considering the recent EXO results).

DOI: 10.1103/PhysRevD.86.113014 PACS numbers: 14.60.Pq, 14.60.Lm, 14.60.St

I. INTRODUCTION

In recent years, several short-baseline neutrino oscillation experiments have found anomalies, which may require an extension of the standard three-neutrino mixing framework, which describes the neutrino oscillations observed in solar, atmospheric, and long-baseline experiments (see Refs. [1–3]). In this paper, we consider the Gallium anomaly [4–6] and the reactor anomaly [7–9], which indicate that electron neutrino and antineutrinos may disappear at short distances.[1] Such disappearance may be explained by the presence of at least one massive neutrino at the eV scale, which drives short-baseline neutrino oscillations generated by a squared-mass difference, which is much larger than the squared-mass difference operating in the solar, atmospheric, and long-baseline neutrino oscillation experiments. We consider 3 + 1 neutrino mixing, which is the minimal extension of three-neutrino mixing, which can explain the Gallium and reactor anomalies. Since from the LEP measurement of the invisible width of the Z boson [13] we know that there are only three light active flavor neutrinos, the additional neutrino in the 3 + 1 framework is sterile.

In this paper, we discuss the implications of the recent ^{71}Ga(^{3}He, ^{3}H)^{71}Ge measurement in Ref. [14], which give information on the neutrino cross section in Gallium experiments. We take also into account the most updated calculation of the reactor neutrino fluxes presented in the recent white paper on light sterile neutrinos [15]. We present also a detailed discussion of the connection between the results of the fit of neutrino oscillation data and the results of β-decay experiments (considering the Mainz data presented very recently in Ref. [16]) and neutrinoless double-β decay experiments (considering the recent EXO bound in Ref. [17] and the controversial positive result in Ref. [18]).

We consider 3 + 1 neutrino mixing as an extension of standard three-neutrino mixing. The mixing of the three active flavor neutrino fields ν_e, ν_μ, ν_τ and one sterile neutrino field ν_s is given by

$$\nu_\alpha = \sum_{k=1}^{4} U_{\alpha k}\nu_k, \tag{1}$$

where U is the unitary 4×4 mixing matrix ($U^\dagger = U^{-1}$) and each of the four ν_k's is a massive neutrino field with mass m_k. We consider the squared-mass hierarchy

$$\Delta m^2_{21} \ll \Delta m^2_{31} \ll \Delta m^2_{41}, \tag{2}$$

with $\Delta m^2_{kj} \equiv m^2_k - m^2_j$, such that Δm^2_{21} generates the very-long-baseline oscillations observed in solar neutrino experiments and in the KamLAND reactor antineutrino experiment, Δm^2_{31} generates the long-baseline oscillations observed in atmospheric neutrino experiments and in long-baseline accelerator and reactor neutrino and

[1]The inclusion in the analysis of the more controversial LSND [10] and MiniBooNE [11] $\overset{(-)}{\nu}_\mu \to \overset{(-)}{\nu}_e$ anomalies will be discussed elsewhere [12].

antineutrino experiments, and Δm^2_{41} generates short-baseline oscillations.

The effective survival probability at a distance L of electron neutrinos and antineutrinos with energy E in short-baseline neutrino oscillation experiments is given by (see Refs. [19–22])

$$P^{\mathrm{SBL}}_{\overset{(-)}{\nu}_e\to\overset{(-)}{\nu}_e} = 1 - \sin^2 2\vartheta_{ee}\sin^2\left(\frac{\Delta m^2_{41}L}{4E}\right), \quad (3)$$

with the transition amplitude

$$\sin^2 2\vartheta_{ee} = 4|U_{e4}|^2(1 - |U_{e4}|^2). \quad (4)$$

The plan of the paper is as follows. In Sec. II, we discuss in detail the Gallium ν_e anomaly [4–6] and the implications of the important recent ^{71}Ga(^{3}He, ^{3}H)^{71}Ge measurement in Ref. [14]. In Sec. III, we present the results of the combined analysis of Gallium data with reactor $\bar{\nu}_e$ data, taking into account the reactor $\bar{\nu}_e$ anomaly [7–9,15]. In Sec. IV, we discuss the solar neutrino constraint on short-baseline ν_e disappearance [23–26]. In Sec. V, we present the results of the global fit of ν_e and $\bar{\nu}_e$ disappearance data, which includes also $\nu_e + {}^{12}\mathrm{C} \to {}^{12}\mathrm{N}_{\mathrm{g.s.}} + e^-$ scattering data [27,28]. We confront these results with the bounds on the heavy neutrino mass given by the data of β-decay experiments [16,29] and neutrinoless double-β decay experiments [17,18]. Finally, in Sec. VI, we draw our conclusions.

II. GALLIUM ANOMALY

The GALLEX [30–32] and SAGE [33–36] Gallium solar neutrino experiments have been tested with intense artificial ^{51}Cr and ^{37}Ar radioactive sources, which produce electron neutrinos through electron capture with the energies and branching ratios given in Table I. In each of these experiments, the source was placed near the center of the approximately cylindrical detector and electron neutrinos have been detected with the solar neutrino detection reaction

$$\nu_e + {}^{71}\mathrm{Ga} \to {}^{71}\mathrm{Ge} + e^-. \quad (5)$$

The average neutrino traveling distances are $\langle L\rangle_{\mathrm{GALLEX}} = 1.9$ m and $\langle L\rangle_{\mathrm{SAGE}} = 0.6$ m. The first line in Table II shows the ratios R_{B} of measured and expected ^{71}Ge event rates reported by the experimental collaborations. The index B indicates that the expected event rates have been calculated using the Bahcall cross sections [37]

TABLE I. Energy (E) and branching ratio (BR) of the neutrino lines produced in the electron-capture decay of ^{51}Cr and ^{37}Ar.

	^{51}Cr				^{37}Ar	
E[keV]	747	752	427	432	811	813
BR	0.8163	0.0849	0.0895	0.0093	0.902	0.098

TABLE II. Ratios of measured and expected ^{71}Ge event rates in the four radioactive source experiments. G1 and G2 denote the two GALLEX experiments with ^{51}Cr sources [30–32], S1 denotes the SAGE experiment with a ^{51}Cr source, and S2 denotes the SAGE experiment with a ^{37}Ar source [33–36]. AVE denotes the weighted average.

	G1	G2	S1	S2	AVE
R_{B}	$0.95^{+0.11}_{-0.11}$	$0.81^{+0.10}_{-0.11}$	$0.95^{+0.12}_{-0.12}$	$0.79^{+0.08}_{-0.08}$	$0.86^{+0.05}_{-0.05}$
R_{HK}	$0.85^{+0.12}_{-0.12}$	$0.71^{+0.11}_{-0.11}$	$0.84^{+0.13}_{-0.12}$	$0.71^{+0.09}_{-0.09}$	$0.77^{+0.08}_{-0.08}$
R_{FF}	$0.93^{+0.11}_{-0.11}$	$0.79^{+0.10}_{-0.11}$	$0.93^{+0.11}_{-0.12}$	$0.77^{+0.09}_{-0.07}$	$0.84^{+0.05}_{-0.05}$
R_{HF}	$0.83^{+0.13}_{-0.11}$	$0.71^{+0.11}_{-0.11}$	$0.83^{+0.13}_{-0.12}$	$0.69^{+0.10}_{-0.09}$	$0.75^{+0.09}_{-0.07}$

$$\sigma_{\mathrm{B}}({}^{51}\mathrm{Cr}) = 58.1 \times 10^{-46}\ \mathrm{cm}^2, \quad (6)$$

$$\sigma_{\mathrm{B}}({}^{37}\mathrm{Ar}) = 70.0 \times 10^{-46}\ \mathrm{cm}^2, \quad (7)$$

without considering their uncertainties. One can see that the values of $R^{\mathrm{G1}}_{\mathrm{B}}$ and $R^{\mathrm{S1}}_{\mathrm{B}}$ indicate a compatibility between the measured and expected event rates, whereas the values of $R^{\mathrm{G2}}_{\mathrm{B}}$ and $R^{\mathrm{S2}}_{\mathrm{B}}$ are significantly smaller than one, indicating a disappearance of electron neutrinos. The weighted average in Table II gives a 2.7σ anomaly.

Since the values of the cross sections of ^{51}Cr and ^{37}Ar electron neutrinos and their uncertainties are crucial for the interpretation of the Gallium data as indication of short-baseline ν_e disappearance, in the following we discuss in detail the problem of the determination of the cross sections and their uncertainties, taking into account Refs. [37–40] and the important recent measurement in Ref. [14].

The cross sections of the interaction process (5) for neutrinos produced by ^{51}Cr and ^{37}Ar sources are given by

$$\sigma = \sigma_{\mathrm{gs}}\left(1 + \xi_{175}\frac{\mathrm{BGT}_{175}}{\mathrm{BGT}_{\mathrm{gs}}} + \xi_{500}\frac{\mathrm{BGT}_{500}}{\mathrm{BGT}_{\mathrm{gs}}}\right), \quad (8)$$

where σ_{gs} is the cross section of the transitions from the ground state of ^{71}Ga to the ground state of ^{71}Ge, $\mathrm{BGT}_{\mathrm{gs}}$ is the corresponding Gamow-Teller strength (BGT), and BGT_{175} and BGT_{500} are the Gamow-Teller strengths of the transitions from the ground state of ^{71}Ga to the two excited states of ^{71}Ge at about 175 and 500 keV (see Fig. 1). The coefficients of $\mathrm{BGT}_{175}/\mathrm{BGT}_{\mathrm{gs}}$ and $\mathrm{BGT}_{500}/\mathrm{BGT}_{\mathrm{gs}}$

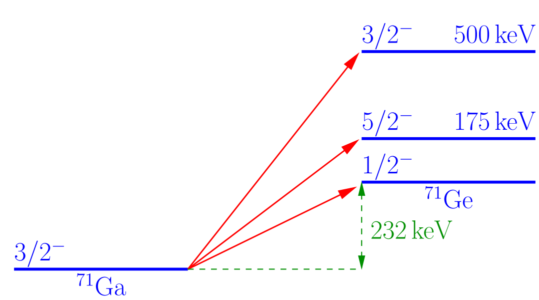

FIG. 1 (color online). ^{71}Ga $\to$ ^{71}Ge transitions induced by ^{51}Cr and ^{37}Ar electron neutrinos.

are determined by phase space: $\xi_{175}(^{51}\mathrm{Cr}) = 0.669$, $\xi_{500}(^{51}\mathrm{Cr}) = 0.220$, $\xi_{175}(^{37}\mathrm{Ar}) = 0.695$, $\xi_{500}(^{37}\mathrm{Ar}) = 0.263$ [37].

The cross sections of the transitions from the ground state of ^{71}Ga to the ground state of ^{71}Ge have been calculated accurately by Bahcall [37],

$$\sigma_{\mathrm{gs}}(^{51}\mathrm{Cr}) = 55.3 \times 10^{-46}\ \mathrm{cm}^2, \tag{9}$$

$$\sigma_{\mathrm{gs}}(^{37}\mathrm{Ar}) = 66.2 \times 10^{-46}\ \mathrm{cm}^2. \tag{10}$$

These cross sections are proportional to the characteristic neutrino absorption cross section [37,41]

$$\begin{aligned}\sigma_0 &= 2\alpha Z_{\mathrm{Ge}} m_e^2 G_{\mathrm{F}}^2 |V_{ud}|^2 g_A^2 \mathrm{BGT}_{\mathrm{gs}} \\ &= Z_{\mathrm{Ge}} \mathrm{BGT}_{\mathrm{gs}} (3.091 \pm 0.012) \times 10^{-46}\ \mathrm{cm}^2,\end{aligned} \tag{11}$$

where α is the fine-structure constant, $Z_{\mathrm{Ge}} = 32$ is the atomic number of the final nucleus, m_e is the electron mass, G_{F} is the Fermi constant, V_{ud} is the ud element of the quark mixing matrix V, and g_A is the axial coupling constant. The numerical value of the coefficient in the last line of Eq. (11) has been obtained with the values of these quantities given in the last Review of Particle Physics [42]. From the value

$$\sigma_0 = (8.611 \pm 0.011) \times 10^{-46}\ \mathrm{cm}^2, \tag{12}$$

calculated by Bahcall [37] using the accurate measurement [43]

$$T_{1/2}(^{71}\mathrm{Ge}) = 11.43 \pm 0.03\ d \tag{13}$$

of the lifetime of ^{71}Ge [which decays through the electron-capture process $e^- + {}^{71}_{32}\mathrm{Ge} \to {}^{71}_{31}\mathrm{Ga} + \nu_e$, which is the inverse of the ν_e detection process (5)], we obtain

$$\mathrm{BGT}_{\mathrm{gs}} = 0.0871 \pm 0.0004. \tag{14}$$

This value agrees with that given in Ref. [40], but it is different from that recommended in Ref. [14]. Hence, we checked it using the relation

$$\begin{aligned}\mathrm{BGT}_{\mathrm{gs}} &= \frac{[2J_{\mathrm{Ge}} + 1]}{[2J_{\mathrm{Ga}} + 1]} \frac{2\pi^3 \ln 2}{G_{\mathrm{F}}^2 |V_{ud}|^2 m_e^5 g_A^2 f t_{1/2}(^{71}\mathrm{Ge})} \\ &= \frac{6289 \pm 3\ \mathrm{s}}{2 g_A^2 f t_{1/2}(^{71}\mathrm{Ge})},\end{aligned} \tag{15}$$

with $J_{\mathrm{Ge}} = 1/2$ and $J_{\mathrm{Ga}} = 3/2$, and the value

$$\log f t_{1/2}(^{71}\mathrm{Ge}) = 4.3493 \pm 0.0015, \tag{16}$$

obtained with the LOGFT calculator [44] of the National Nuclear Data Center using the lifetime (13). The result,

$$\mathrm{BGT}_{\mathrm{gs}} = 0.0872 \pm 0.0005, \tag{17}$$

is in agreement with the value (14), which will be used in the following.

The Gamow-Teller strengths BGT_{175} and BGT_{500} have been measured in 1985 in the (p, n) experiment of Krofcheck *et al.* [38,39] and recently, in 2011, in the $(^3\mathrm{He}, {}^3\mathrm{H})$ experiment of Frekers *et al.* [14]. The results are listed in Table III together with the 1998 shell-model calculation of BGT_{175} of Haxton [40].

The Bahcall cross sections (6) and (7) have been obtained using for BGT_{500} the Krofcheck *et al.* measurement and for BGT_{175} half of the Krofcheck *et al.* upper limit [37].

In previous publications [6,28,45–48] we used the Haxton shell-model value of BGT_{175} and the (p, n) measured value of BGT_{500}. Although the uncertainties of the Haxton shell-model value of BGT_{175} are so large that BGT_{175} may be negligibly small, the central value is much larger than the upper limit obtained in the (p, n) experiment. According to Ref. [40], this is due to a suppression of the (p, n) value caused by a destructive interference between the spin $(\Delta J = 1,\ \Delta L = 0)$ matrix element and an additional spin-tensor $(\Delta J = 1, \Delta L = 2)$ matrix element which operates only in (p, n) transitions. We do not know if the same suppression is operating also in $(^3\mathrm{He}, {}^3\mathrm{H})$, which could be the explanation of the smallness of the value of BGT_{175} measured by Frekers *et al.*, which is compatible with the (p, n) upper bound. Moreover, the value of BGT_{500} measured by Frekers *et al.* has a 2.7σ discrepancy with that measured by Krofcheck *et al.* Since we cannot solve these problems, we consider the following three approaches which give the cross sections in Table IV and the ratios of measured and expected ^{71}Ge event rates in Table II:

HK Haxton BGT_{175} value and Krofcheck *et al.* BGT_{500} value. This is our old approach adopted in previous publications [6,28,45–48]. The cross sections are significantly larger than the Bahcall cross sections in Eqs. (6) and (7), albeit with large uncertainties, which make them compatible at the 1σ level.

TABLE III. Values of the Gamow-Teller strengths of the transitions from the ground state of ^{71}Ga to the two excited states of ^{71}Ge at 175 and 500 keV and their relative values with respect to the Gamow-Teller strength of the transitions to the ground state of ^{71}Ge, given in Eq. (14).

Reference	Method	BGT_{175}	$\frac{\mathrm{BGT}_{175}}{\mathrm{BGT}_{\mathrm{gs}}}$	BGT_{500}	$\frac{\mathrm{BGT}_{500}}{\mathrm{BGT}_{\mathrm{gs}}}$
Krofcheck *et al.* [38,39]	$^{71}\mathrm{Ga}(p, n)^{71}\mathrm{Ge}$	<0.005	<0.057	0.011 ± 0.002	0.126 ± 0.023
Haxton [40]	shell Model	0.017 ± 0.015	0.19 ± 0.18		
Frekers *et al.* [14]	$^{71}\mathrm{Ga}(^3\mathrm{He}, {}^3\mathrm{H})^{71}\mathrm{Ge}$	0.0034 ± 0.0026	0.039 ± 0.030	0.0176 ± 0.0014	0.202 ± 0.016

TABLE IV. Gallium cross section (in units of 10^{-46} cm^2) and its ratio with the corresponding Bahcall cross section [Eqs. (6) and (7)] for ^{51}Cr and ^{37}Ar neutrinos in the three cases discussed in the text.

	^{51}Cr		^{37}Ar	
	σ	σ/σ_B	σ	σ/σ_B
HK	63.9 ± 6.5	1.10 ± 0.11	77.2 ± 8.1	1.10 ± 0.12
FF	59.2 ± 1.1	1.02 ± 0.02	71.5 ± 1.4	1.02 ± 0.02
HF	64.9 ± 6.5	1.12 ± 0.11	78.5 ± 8.1	1.12 ± 0.12

FF Frekers *et al.* values of both BGT$_{175}$ and BGT$_{500}$. This is a new approach, which is motivated by the new (^{3}He, ^{3}H) measurements [14]. The cross sections are only slightly larger than the Bahcall cross sections in Eqs. (6) and (7), mainly because of the larger BGT$_{500}$.

HF Haxton BGT$_{175}$ value and Frekers *et al.* BGT$_{500}$ value. This is a new approach, which is motivated by the possibility that the BGT$_{175}$ measured by Frekers *et al.* suffers of destructive interference between the spin and spin-tensor matrix element and its value is different from the BGT$_{175}$ in Gallium neutrino detection, as discussed by Haxton for the (p, n) experiment [40]. This approach gives the largest cross sections, which however are still compatible with the Bahcall cross sections at the 1σ level.

From the weighted averages of measured and expected ^{71}Ge event rates in Table II it follows that the statistical significance of the Gallium anomaly in the three cases is, respectively, about 3.0σ, 2.9σ, and 3.1σ. Hence, the new (^{3}He, ^{3}H) cross section measurement of Frekers *et al.* [14] confirm that there is a Gallium anomaly at a level of about 3σ [6], which indicates a short-baseline disappearance of ν_e, which can be explained by neutrino oscillations.

We analyzed the Gallium data in the three cases above in terms of neutrino oscillations in the 3 + 1 framework, in which the effective probability of ν_e survival is given by Eq. (3) with $\alpha = e$. We used the statistical method discussed in Ref. [6], neglecting for simplicity the small difference between the ^{51}Cr and ^{37}Ar cross section ratios in Table IV. The results of the fits are presented in Table V and Figs. 2–4. One can see that in any case neutrino

TABLE V. Values of χ^2, goodness of fit (GoF) for 2 degrees of freedom and best-fit values of the 3 + 1 oscillation parameters obtained from the three fits of Gallium data described in the text.

	HK	FF	HF
$\chi^2_{\rm min}$	4.8	7.9	4.6
GoF	9.1%	1.9%	9.9%
Δm^2_{41}[eV^2]	2.24	2.1	2.24
$\sin^2 2\vartheta_{ee}$	0.50	0.30	0.52

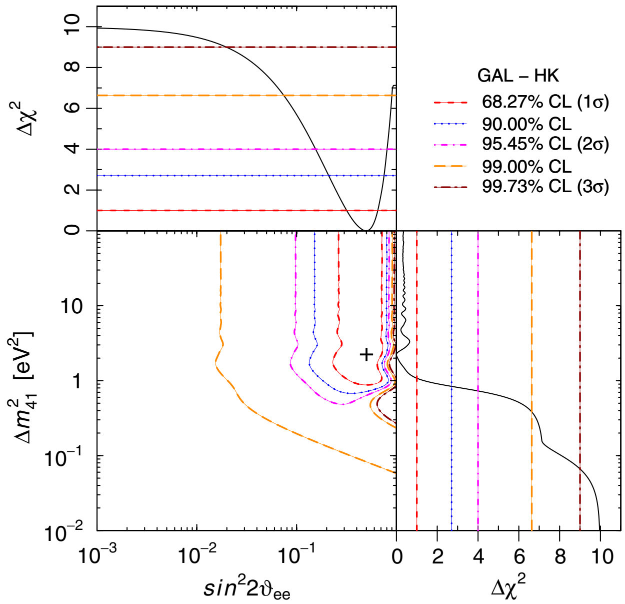

FIG. 2 (color online). Allowed regions in the $\sin^2 2\vartheta_{ee} - \Delta m^2_{41}$ plane and marginal $\Delta\chi^2$'s for $\sin^2 2\vartheta_{ee}$ and Δm^2_{41} obtained from the combined fit of the results of the Gallium radioactive source experiments in the HK case (see the text). The best-fit point corresponding to $\chi^2_{\rm min}$ is indicated by a cross.

oscillations give an acceptable fit of the data. In the FF case the goodness of fit is smaller than in the HK and HF cases, because of the much smaller uncertainty of BGT$_{175}$. The three cases give approximately the same best-fit value and allowed range of Δm^2_{41}. Instead, they differ in the best-fit value and allowed range of $\sin^2 2\vartheta_{ee}$: the FF case is in

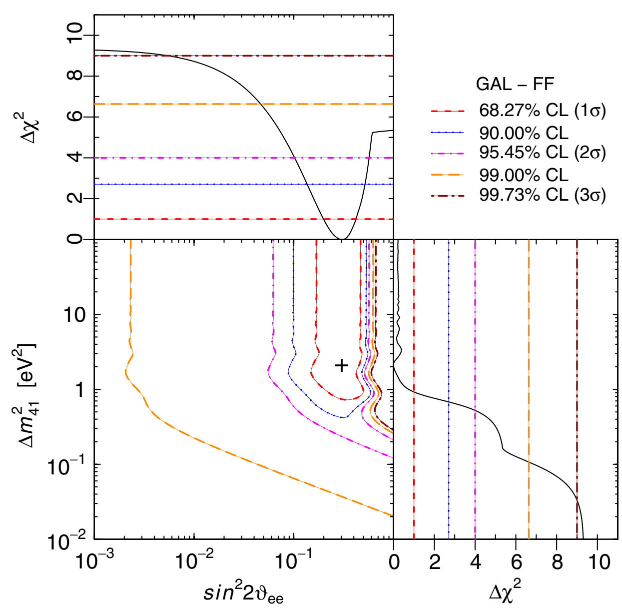

FIG. 3 (color online). Allowed regions and marginal $\Delta\chi^2$'s analogous to those in Fig. 2 for the FF case.

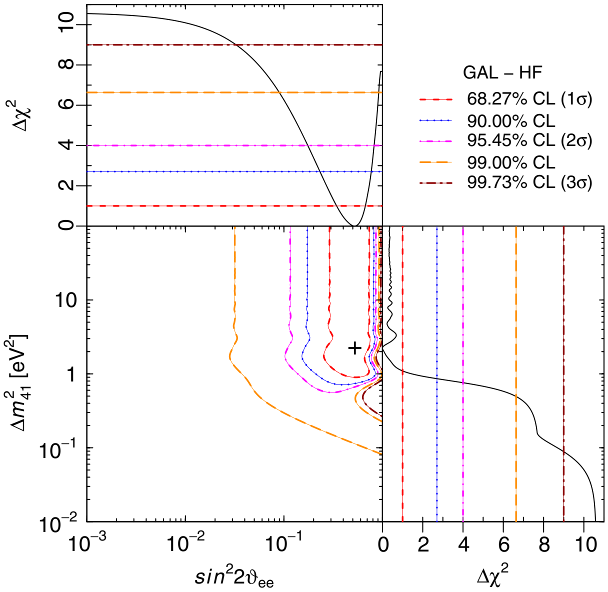

FIG. 4 (color online). Allowed regions and marginal $\Delta\chi^2$'s analogous to those in Fig. 2 for the HF case.

favor of smaller values of $\sin^2 2\vartheta_{ee}$ than the HK and HF cases.

III. FIT OF GALLIUM AND REACTOR DATA

The reactor antineutrino anomaly [9] stems from a new evaluation of the reactor $\bar{\nu}_e$ flux [7,8], which implies that the event rate measured by several reactor $\bar{\nu}_e$ experiments at distances from the reactor core between about 10 and 100 meters is smaller than that obtained without $\bar{\nu}_e$ disappearance. This is illustrated in Fig. 5, where we plotted the ratio R of the observed $\bar{\nu}_e$ event rate and that expected in absence of $\bar{\nu}_e$ disappearance for the Bugey-3 [49], Bugey-4 [50], ROVNO91 [51], Gosgen [52], ILL [53], and Krasnoyarsk [54] reactor antineutrino experiments. We used the reactor neutrino fluxes presented in the recent white paper on light sterile neutrinos [15], which updates Refs. [7–9]. From Fig. 5, one can see that the reactor antineutrino anomaly has a significance of about 2.8σ. In the fit of reactor data, besides the above-mentioned rates, we consider also the 40 m/15 m spectral ratio measured in the Bugey-3 experiment [49].

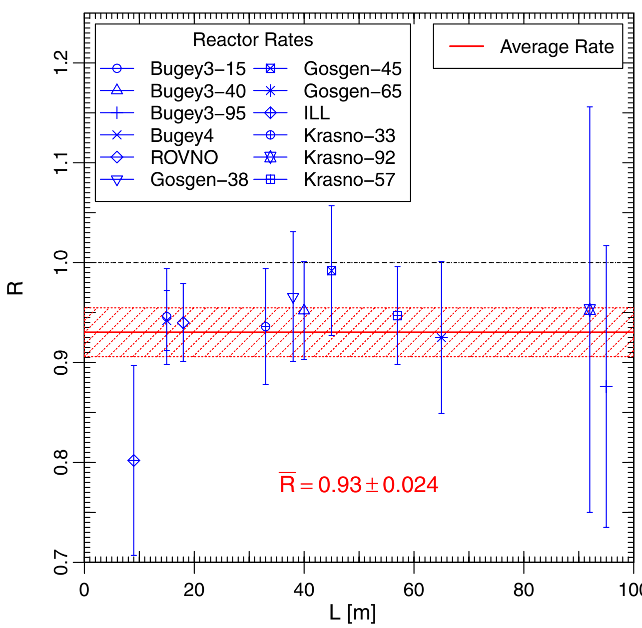

FIG. 5 (color online). Ratio R of the observed $\bar{\nu}_e$ event rate and that expected in absence of $\bar{\nu}_e$ disappearance in reactor neutrino experiments. The horizontal band represents the average value of R with 1σ uncertainties.

TABLE VI. Values of χ^2, number of degrees of freedom (NDF), goodness of fit (GoF), and best-fit values of the 3 + 1 oscillation parameters obtained from the fit of reactor (REA) antineutrino data (first column) and from the combined fit of reactor and Gallium data in the three cases discussed in Sec. II. The last three lines give the parameter goodness of fit (PG) [55] of the combined fit.

	REA	REA + HK	REA + FF	REA + HF
$\chi^2_{\min}$	21.5	30.6	31.8	31.0
NDF	36	40	40	40
GoF	97%	86%	82%	85%
$\Delta m^2_{41}[\mathrm{eV}^2]$	1.9	1.95	1.95	1.95
$\sin^2 2\vartheta_{ee}$	0.13	0.16	0.16	0.16
$\Delta\chi^2_{\mathrm{PG}}$		4.3	2.4	4.8
$\mathrm{NDF}_{\mathrm{PG}}$		2	2	2
$\mathrm{GoF}_{\mathrm{PG}}$		12%	30%	9%

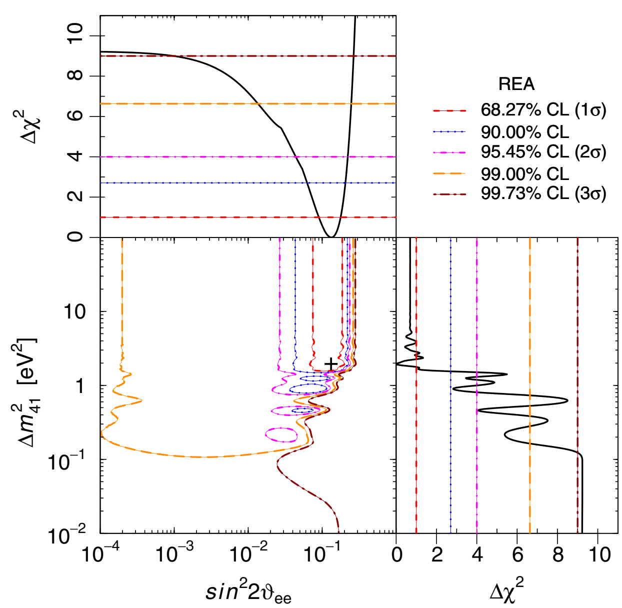

FIG. 6 (color online). Allowed regions in the $\sin^2 2\vartheta_{ee} - \Delta m^2_{41}$ plane and marginal $\Delta\chi^2$'s for $\sin^2 2\vartheta_{ee}$ and Δm^2_{41} obtained from the combined fit of reactor antineutrino data. The best-fit point corresponding to $\chi^2_{\min}$ is indicated by a cross.

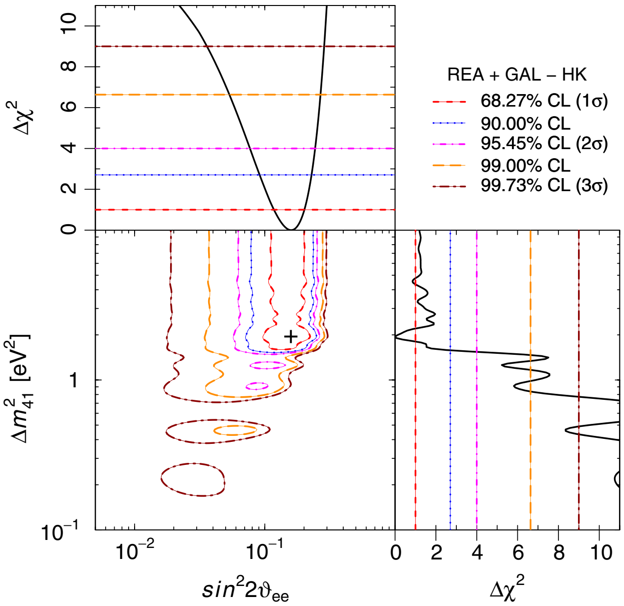

FIG. 7 (color online). Allowed regions in the $\sin^2 2\vartheta_{ee} - \Delta m^2_{41}$ plane and marginal $\Delta\chi^2$'s for $\sin^2 2\vartheta_{ee}$ and Δm^2_{41} obtained from the combined fit of Gallium and reactor data in the HF case discussed in Sec. II. The best-fit point corresponding to $\chi^2_{\rm min}$ is indicated by a cross.

The results of the fit of the reactor antineutrino data are presented in Table VI and Fig. 6. One can see that the preferred range of Δm_{41} has a large overlap with that indicated by the Gallium anomaly, but there is a strong upper bound for $\sin^2 2\vartheta_{ee}$ of about 0.3. Therefore, the large-$\sin^2 2\vartheta_{ee}$ part of the Gallium-allowed region in each

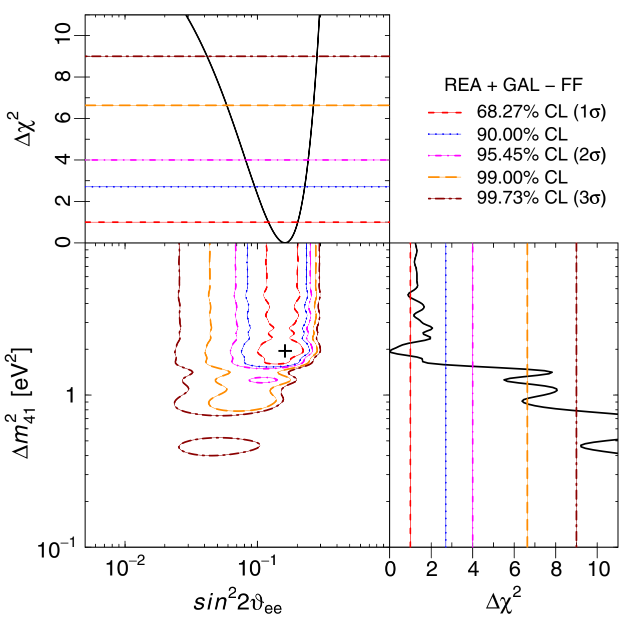

FIG. 8 (color online). Allowed regions and marginal $\Delta\chi^2$'s analogous to those in Fig. 7 for the FF case.

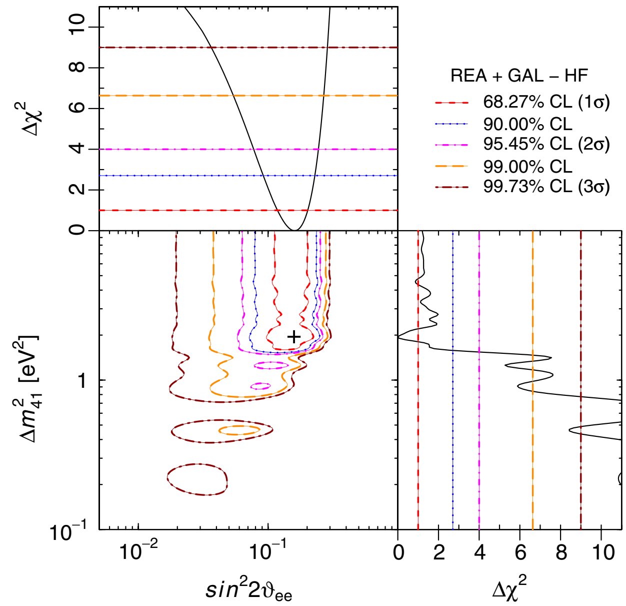

FIG. 9 (color online). Allowed regions and marginal $\Delta\chi^2$'s analogous to those in Fig. 7 for the HF case.

of the three cases considered in Figs. 2–4 is excluded by reactor data.

The results of the combined fit of Gallium and reactor data are presented in Table VI and Figs. 7–9. From these figures, one can see that the allowed regions in the $\sin^2 2\vartheta_{ee} - \Delta m^2_{41}$ in the three cases that we have considered for the fit of Gallium data are quite similar, and the best-fit values of $\sin^2 2\vartheta_{ee}$ and Δm^2_{41} are equal (see Table VI). This is due to a dominance of reactor data, which are more numerous and have smaller uncertainties. Hence, in the following we consider only the FF case, which is the one which is more compatible with reactor data, because it agrees more than the HK and HF cases with the reactor exclusion of large values of $\sin^2 2\vartheta_{ee}$. This better agreement is quantified by the larger parameter goodness of fit [55] in Table VI.

IV. SOLAR NEUTRINO CONSTRAINT

In this section, we discuss the upper bound for $\sin^2 2\vartheta_{ee}$, which can be obtained from the data of solar neutrino experiments [32,56–66] and from the data of the KamLAND very-long-baseline reactor antineutrino experiment [67], which is sensitive to oscillations generated by the small squared-mass difference Δm^2_{21}. Since the event rates measured in these experiments are well described by standard three-neutrino mixing, the data allow us to constrain the corrections due to active-sterile neutrino mixing, which affects the electron neutrino and antineutrino survival probability and generates transitions into sterile neutrinos [23–26,68,69]. As explained in the following, the almost degenerate effects in the solar and KamLAND experiments [24–26] of $|U_{e4}|^2$, which determine $\sin^2 2\vartheta_{ee}$ through Eq. (4), and $|U_{e3}|^2$ can be resolved by using the recent determination of $|U_{e3}|^2$ in the Daya Bay [70] and RENO [71] long-baseline reactor antineutrino experiments.

The effective survival probability of electron neutrinos and antineutrinos in the solar and KamLAND experiments is given by[2] [72]

$$P^{\rm SUN}_{\nu_e\to\nu_e} = P^{2\nu}_{\nu_e\to\nu_e}\left(1-\sum_{k=3}^{4}|U_{ek}|^2\right)^2 + \sum_{k=3}^{4}|U_{ek}|^4, \quad (18)$$

where $P^{2\nu}_{\nu_e\to\nu_e}$ is the two-neutrino survival probability generated by Δm^2_{21}. Considering small values of $|U_{e3}|^2$ and $|U_{e4}|^2$, we have

$$P^{\rm SUN}_{\nu_e\to\nu_e} \simeq P^{2\nu}_{\nu_e\to\nu_e}\left(1-2\sum_{k=3}^{4}|U_{ek}|^2\right). \quad (19)$$

In vacuum, the two-neutrino survival probability $P^{2\nu}_{\nu_e\to\nu_e}$ has the standard two-neutrino form which does not depend on $|U_{e3}|^2$ and $|U_{e4}|^2$. Therefore, in the KamLAND experiment $|U_{e3}|^2$ and $|U_{e4}|^2$ have the same effect of suppressing the electron neutrino and antineutrino survival probability. For solar neutrinos, the main effect of $|U_{e3}|^2$ and $|U_{e4}|^2$ is the same as in the vacuum case, but there are corrections caused by the modifications of $P^{2\nu}_{\nu_e\to\nu_e}$ due to the decrease of $|U_{e1}|^2 + |U_{e2}|^2 = 1 - (|U_{e3}|^2 + |U_{e4}|^2)$ if $|U_{e3}|^2 \neq 0$ and/or $|U_{e4}|^2 \neq 0$ and to the contribution of the neutral-current potential $V_{\rm NC}$ which is not felt by the sterile neutrino during propagation in matter.

In order to describe this effect, we neglect possible CP-violating phases in the mixing matrix and we parametrize it as (see also Ref. [24])

$$U = R_{23}R_{24}R_{34}R_{14}R_{13}R_{12}, \quad (20)$$

where R_{ab} is the real orthogonal matrix ($R^T_{ab} = R^{-1}_{ab}$), which operates a rotation in the a-b plane by an angle ϑ_{ab},

$$[R^{ab}]_{rs} = \delta_{rs} + (c_{ab}-1)(\delta_{ra}\delta_{sa}+\delta_{rb}\delta_{sb}) + s_{ab}(\delta_{ra}\delta_{sb}-\delta_{rb}\delta_{sa}), \quad (21)$$

with $c_{ab} \equiv \cos\vartheta_{ab}$ and $s_{ab} \equiv \sin\vartheta_{ab}$. In this parametrization, the electron line of the mixing matrix is given by

$$U_{e1} = c_{12}c_{13}c_{14}, \qquad U_{e2} = s_{12}c_{13}c_{14}, \quad (22)$$

$$U_{e3} = s_{13}c_{14}, \qquad U_{e4} = s_{14}. \quad (23)$$

Hence, this is an extension of the standard three-neutrino mixing parametrization of the electron line (see Refs. [1–3]) with the addition of ν_e-ν_4 mixing parametrized by ϑ_{14}. This parametrization is also convenient because

$$\vartheta_{ee} = \vartheta_{14}. \quad (24)$$

Since the sterile line of the mixing matrix is more complicated, it is convenient to write its first two elements as

$$U_{s1} = \cos\varphi_s\cos\chi_s, \qquad U_{s2} = \sin\varphi_s\cos\chi_s, \quad (25)$$

with

$$\tan\varphi_s = \frac{Zs_{12}c_{24}+c_{12}s_{24}}{Zc_{12}c_{24}-s_{12}s_{24}}, \quad (26)$$

$$\cos^2\chi_s = 1-\sum_{k=3}^{4}|U_{sk}|^2 = Z^2c^2_{24}+s^2_{24}, \quad (27)$$

$$Z = c_{13}c_{34}s_{14} - s_{13}s_{34}. \quad (28)$$

The adiabatic two-neutrino survival probability $P^{2\nu}_{\nu_e\to\nu_e}$ is given by [23]

$$P^{2\nu}_{\nu_e\to\nu_e} = \frac{1}{2}(1+\cos2\vartheta_{12}\cos2\vartheta^0_{12}), \quad (29)$$

where ϑ^0_{12} is the effective mixing angle at neutrino production, which is given by

$$\vartheta^0_{12} = \vartheta_{12} + \omega^0. \quad (30)$$

The mixing angle ω between the vacuum mass basis and the effective mass basis in matter is given by

$$\tan2\omega = \frac{2EV\sin2\xi}{\Delta m^2_{21} - 2EV\cos2\xi}. \quad (31)$$

Here V is the matter potential given by

$$V^2 = V^2_{\rm CC}c^4_{13}c^4_{14} + V^2_{\rm NC}\cos^4\chi_s - 2V_{\rm CC}V_{\rm NC}\cos2(\vartheta_{12}-\varphi_s)c^2_{13}c^2_{14}\cos^2\chi_s, \quad (32)$$

where $V_{\rm CC}$ and $V_{\rm NC}$ are the standard charged-current and neutral-current matter potentials. The angle ξ is given by

$$\tan2\xi = \frac{V_{\rm CC}\sin2\vartheta_{12}c^2_{13}c^2_{14} - V_{\rm NC}\sin2\varphi_s\cos^2\chi_s}{V_{\rm CC}\cos2\vartheta_{12}c^2_{13}c^2_{14} - V_{\rm NC}\cos2\varphi_s\cos^2\chi_s}. \quad (33)$$

Therefore, for $s_{14} \ll 1$ the contributions of $|U_{e3}|^2 \simeq s^2_{13}$ and $|U_{e4}|^2 = s^2_{14}$ to the matter effects are almost degenerate. There is only a small difference of their contributions due to Z in Eq. (28).

In solar neutrino measurements the degeneracy of the effects of $|U_{e3}|^2$ and $|U_{e4}|^2$ is also slightly broken by the Sudbury neutrino observatory (SNO) neutral-current measurement, which is sensitive to the total probability of ν_e transitions into active neutrinos, which by unitarity is given by $1 - P^{\rm SUN}_{\nu_e\to\nu_s}$, with

$$P^{\rm SUN}_{\nu_e\to\nu_s} = P^{2\nu}_{\nu_e\to\nu_s}c^2_{13}c^2_{14}\cos^2\chi_s + \sum_{k=3}^{4}|U_{ek}|^2|U_{sk}|^2. \quad (34)$$

Here, the adiabatic two-neutrino transition probability $P^{2\nu}_{\nu_e\to\nu_s}$ is given by[3] [23]

[2] In this discussion we neglect, for simplicity, the matter effects in the Earth, which affect the neutrino detection rates in the night, but these effects are taken into account in our calculation.

[3] One can check that in the limit of two-neutrino ν_e-ν_s mixing the unitarity relation $P^{2\nu}_{\nu_e\to\nu_e} + P^{2\nu}_{\nu_e\to\nu_s} = 1$ is satisfied. In this case, $c_{13} = c_{14} = s_{24} = \cos\chi_s = 1$ and $\varphi_s = \vartheta_{12} + \pi/2$.

$$P^{2\nu}_{\nu_e\to\nu_s} = \frac{1}{2}(1 + \cos 2\varphi_s \cos 2\vartheta^0_{12}). \tag{35}$$

The degeneracy of $|U_{e3}|^2$ and $|U_{e4}|^2$ is broken by their different effects in φ_s, χ_s and in the last term of Eq. (34).

Luckily, the recent determination of the value of ϑ_{13} in the Daya Bay [70] and RENO [71] experiment allows us to obtain information on the value of $\vartheta_{ee} = \vartheta_{14}$ without much uncertainty due to ϑ_{13}. In the 3 + 1 mixing scheme under consideration the effective long-baseline $\bar{\nu}_e$ survival probability in the Daya Bay and RENO far detectors is given by [73]

$$P^{\mathrm{LBL-F}}_{\bar{\nu}_e\to\bar{\nu}_e} = 1 - c^4_{14}\sin^2 2\vartheta_{13}\sin^2\left(\frac{\Delta m^2_{31}L}{4E}\right) - \frac{1}{2}\sin^2 2\vartheta_{14}, \tag{36}$$

since the oscillations due to $\Delta m^2_{41} \gg \Delta m^2_{31}$ are averaged and the oscillations due to $\Delta m^2_{21} \ll \Delta m^2_{31}$ are negligibly small. This survival probability depends on ϑ_{14}, but the Daya Bay and RENO Collaborations measured the ratio of the probability (36) in the far detectors and the probability (36) with $\Delta m^2_{31}L/4E \ll 1$ in the near detectors,

$$P^{\mathrm{LBL-N}}_{\bar{\nu}_e\to\bar{\nu}_e} = 1 - \frac{1}{2}\sin^2 2\vartheta_{14}. \tag{37}$$

Since the contribution of small values of ϑ_{14} to the measured ratio is of order ϑ^4_{14} [74], in practice the value of ϑ_{13} determined by the Daya Bay and RENO Collaborations with a three-neutrino mixing survival probability is accurate also in the 3 + 1 scheme under consideration. Nevertheless, since we have the possibility, in our analysis we took into account the exact ratio of the far and near survival probabilities (36) and (37) by including the least-squares function χ^2_{LBL} of the far/near relative measurements of Daya Bay and RENO in the total solar and reactor least-squares function

$$\chi^2 = \chi^2_{\mathrm{SOL}} + \chi^2_{\mathrm{KL}} + \chi^2_{\mathrm{LBL}}. \tag{38}$$

For the calculation of the solar least-squares function χ^2_{SOL}, we considered the radiochemical ^{37}Cl [56] and ^{71}Ga [32,57] experiments, the day and night energy spectra of all four phases of Super-Kamiokande [58–61], the day and night energy spectra of the SNO D_2O phase [62], the charged-current and neutral-current rates of the SNO salt [63] and neutral current detection [64] phases, and the rates of low energy ^{7}Be [65] and pep [66] solar neutrinos from the Borexino experiment. We did not use the SNO data obtained with the low energy threshold analysis [75] and those obtained with the combined analysis [76] because both analyses assumed a three-parameter polynomial survival probability, which is not appropriate for the sterile neutrino analysis. The solar neutrino fluxes are taken from the BP2004 [77] standard solar model, except for the normalization of the solar 8B neutrino flux, which is considered as a free parameter determined by the minimization of χ^2 (as usual, because of its large theoretical uncertainties).

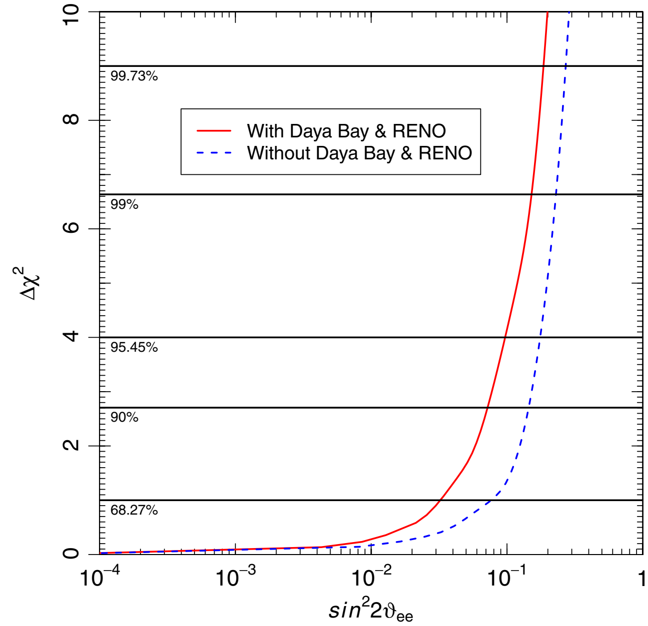

FIG. 10 (color online). Marginalized $\Delta\chi^2 = \chi^2 - \chi^2_{\min}$ as a function of $\sin^2 2\vartheta_{ee}$ obtained from the fit of solar and KamLAND data with and without Daya Bay and RENO data.

The KamLAND least-squares function χ^2_{KL} has been calculated using the energy spectrum reported in Ref. [67] with a total exposure of 3.49×10^{32} target proton year.

In our analysis, we used the ν_e survival probability (18) and the $\nu_e \to \nu_s$ transition probability (34) taking into account as parameters the squared-mass difference Δm^2_{21} and the five relevant mixing angles ϑ_{12}, ϑ_{13}, ϑ_{14}, ϑ_{24}, ϑ_{34} (solar and KamLAND oscillations are independent from ϑ_{23}, because ν_μ and ν_τ are indistinguishable; see Ref. [1]). The six-dimensional parameter space is explored with a Markov chain Monte Carlo sampling in order to minimize the total χ^2 in Eq. (38).

Since the best fit is obtained for $\vartheta_{14} = 0$, the marginalized $\Delta\chi^2 = \chi^2 - \chi^2_{\min}$ shown in Fig. 10 gives stringent constraints on the value of $\sin^2 2\vartheta_{ee} = \sin^2 2\vartheta_{14}$. In Fig. 10 we have plotted the $\Delta\chi^2$ obtained with and without including the Daya Bay and RENO data. One can see that these data are useful in order to tighten the upper bound on $\sin^2 2\vartheta_{ee}$.

V. GLOBAL FIT

In this section, we present the results of the global fit of electron neutrino and antineutrino disappearance data, which includes the Gallium and reactor data discussed respectively in Secs. II and III, the solar neutrino constraint discussed in Sec. IV, and the KARMEN [78,79] and LSND [80] $\nu_e + {}^{12}\mathrm{C} \to {}^{102}\mathrm{N}_{\mathrm{g.s.}} + e^-$ scattering data [27], with the method discussed in Ref. [28].

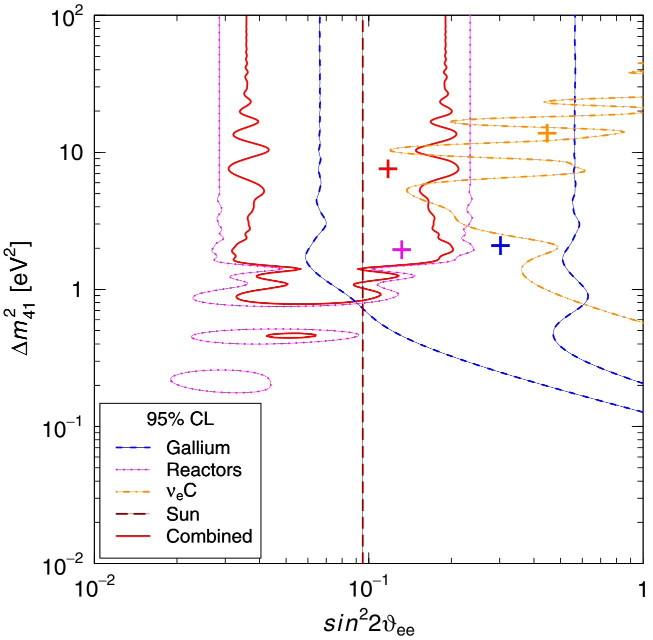

FIG. 11 (color online). Allowed 95% C.L. regions in the $\sin^2 2\vartheta_{ee} - \Delta m^2_{41}$ plane obtained from the separate fits of Gallium, reactor, solar, and ν_eC scattering data and from the combined fit of all data. The best-fit points corresponding to $\chi^2_{\rm min}$ are indicated by crosses.

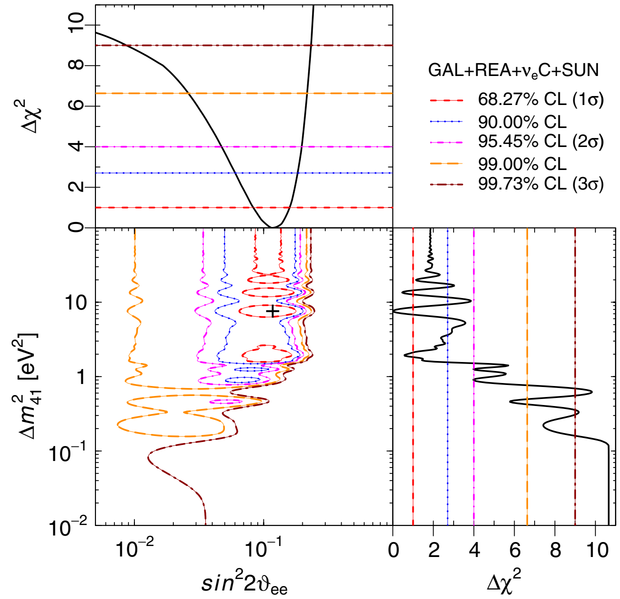

FIG. 12 (color online). Allowed regions in the $\sin^2 2\vartheta_{ee} - \Delta m^2_{41}$ plane and marginal $\Delta\chi^2$'s for $\sin^2 2\vartheta_{ee}$ and Δm^2_{41} obtained from the global fit of ν_e and $\bar{\nu}_e$ data. The best-fit point corresponding to $\chi^2_{\rm min}$ is indicated by a cross.

Figure 11 shows a comparison of the allowed 95% C.L. regions in the $\sin^2 2\vartheta_{ee} - \Delta m^2_{41}$ plane obtained from the separate fits of Gallium, reactor, solar, and ν_eC scattering data and from the combined fit of all data. One can see that the separate allowed regions overlap in a band delimited by $\Delta m^2_{41} \gtrsim 1\ \text{eV}^2$ and $0.07 \lesssim \sin^2 2\vartheta_{ee} \lesssim 0.09$, which is included in the globally allowed 95% C.L. region. Figure 12 shows the globally allowed regions in the $\sin^2 2\vartheta_{ee} - \Delta m^2_{41}$ plane and the marginal $\Delta\chi^2$'s for the two oscillation parameters. The best-fit point is at a relatively large value of Δm^2_{41},

$$(\Delta m^2_{41})_{\rm bf} = 7.6\ \text{eV}^2, \qquad (\sin^2 2\vartheta_{ee})_{\rm bf} = 0.12, \tag{39}$$

with $\chi^2_{\rm min}/\text{NDF} = 45.5/51$, corresponding to a 69% goodness of fit. However, there is a region allowed at 1σ around $\Delta m^2_{41} \simeq 2\ \text{eV}^2$ and $\sin^2 2\vartheta_{ee} \simeq 0.1$. The slight preference of the global fit for $\Delta m^2_{41} \simeq 7.6\ \text{eV}^2$ with respect to $\Delta m^2_{41} \simeq 2\ \text{eV}^2$ (see the marginal $\Delta\chi^2$ for Δm^2_{41} in Fig. 12), which is preferred by Gallium and reactor data (see Tables V and VI and Figs. 2–4 and 6–9), is due to the ν_eC scattering data, which prefer larger values of Δm^2_{41} (see the discussion in Ref. [28]).

Comparing the minimum of the χ^2 of the global fit with the sum of the minima of the χ^2 of the separate fits of Gallium, reactor, solar, and ν_eC scattering data, we obtained $\Delta\chi^2_{\rm PG} = 11.5$, with 5 degrees of freedom, which gives a parameter goodness of fit of 4%. Therefore, the compatibility of the four data sets is acceptable.

The results of the global fit, as well as the results of the fits of Gallium and reactor data, lead to lower limits for Δm^2_{41}, but there is no upper limit for Δm^2_{41} in Figs. 2–4, 6–9, and 12. Hence, one can ask if there are other measurements which constrain large values of Δm^2_{41}. The answer is positive and comes from the measurements of the effects of heavy neutrino masses on electron spectrum in β decay far from the end point, from the results of neutrinoless double-β decay experiments for Majorana neutrinos, and from cosmological measurements. In this discussion we consider the mass hierarchy

$$m_4 \gg m_1, m_2, m_3, \tag{40}$$

which implies

$$m_4 \simeq \sqrt{\Delta m^2_{41}}. \tag{41}$$

Let us consider first β-decay experiments. The ratio of the Kurie function $K(T)$ in β decay for the case of a heavy neutrino ν_4 and that corresponding to massless neutrinos is given by [28]

$$\left(\frac{K(T)}{Q-T}\right)^2 = 1 - |U_{e4}|^2 + |U_{e4}|^2 \sqrt{1 - \frac{m_4^2}{(Q-T)^2}} \times \theta(Q - T - m_4), \tag{42}$$

where T is the kinetic energy of the electron, $Q = 18.574$ keV is the Q value of the decay, θ is the Heaviside step function, and we have neglected the contribution of the three light neutrinos ν_1, ν_2, ν_3. Figure 13 shows the relative deviation of the Kurie plot with respect

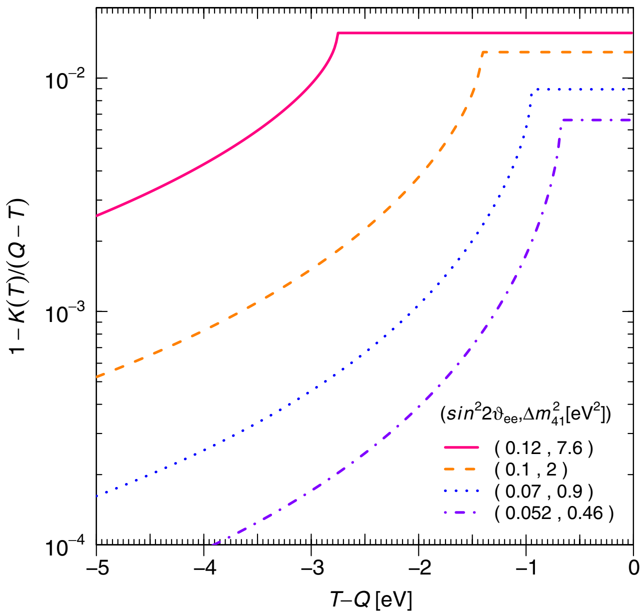

FIG. 13 (color online). Relative deviation of the Kurie plot in β decay for some points in the allowed regions of Fig. 12.

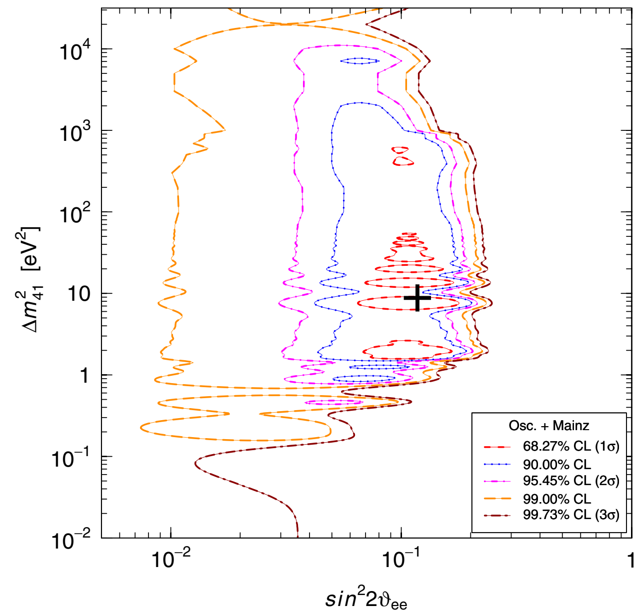

FIG. 15 (color online). Allowed regions in the $\sin^2 2\vartheta_{ee} - \Delta m^2_{41}$ plane obtained from the combined fit of ν_e disappearance and Mainz β-decay data.

to the massless case for some points in the allowed regions of Fig. 12. One can see that in order to see the effect of m_4, β-decay experiments must have a sensitivity to the relative deviation of the Kurie plot of the order of a percent or better for $T \gtrsim Q - m_4$.

In 2001, the Genoa ^{187}Re β-decay experiment [29] searched for deviation of the electron spectrum due to a heavy neutrino with a mass from 50 to 1000 eV. From Fig. 3 of Ref. [29], one can see that the 95% C.L. upper bound for m_4 is about 300 eV if $\sin^2 2\vartheta_{ee} \simeq 0.1$, which implies a very large upper limit on Δm^2_{41} of about 10^5 eV^2.

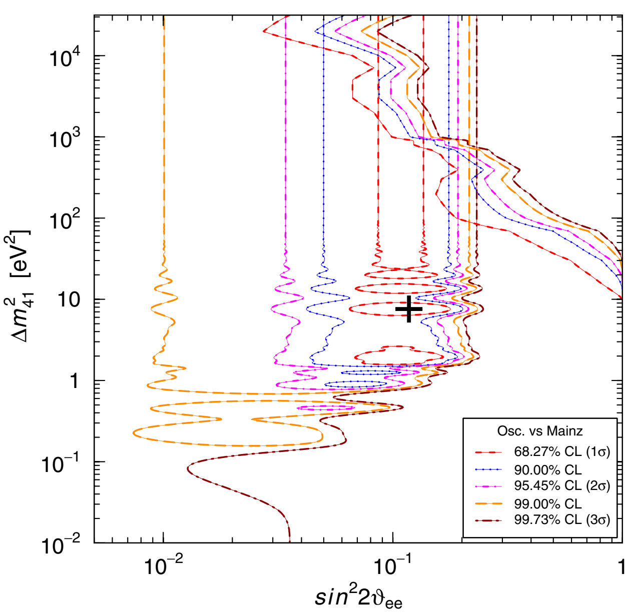

FIG. 14 (color online). Comparison of the Mainz β-decay bound (curves in the top-right part of the figure) with the allowed regions in the $\sin^2 2\vartheta_{ee} - \Delta m^2_{41}$ plane obtained from the global fit of ν_e disappearance data (same as in Fig. 12).

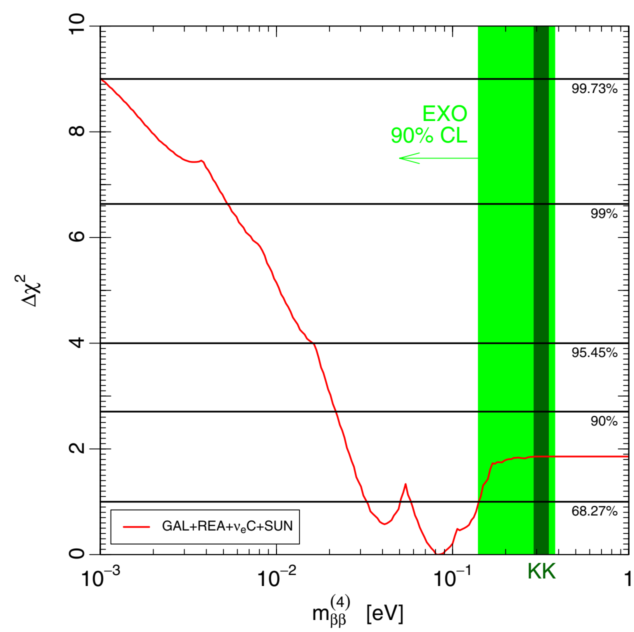

FIG. 16 (color online). Marginal $\Delta\chi^2 = \chi^2 - \chi^2_{\rm min}$ as a function of $m^{(4)}_{\beta\beta}$ obtained from the global fit. The vertical shaded band represents the currently most stringent 90% C.L. upper bound for $m^{(4)}_{\beta\beta}$ in the no-cancellation case (47) obtained from the 90% C.L. EXO bound on $m_{\beta\beta}$ taking into account nuclear matrix element uncertainties [17]. The vertical dark shaded (dark green) band corresponds to the 1σ Klapdor-Kleingrothaus *et al.* range of $m_{\beta\beta}$ [18].

Very recently, the Mainz Collaboration released new data obtained with the phase II of the Mainz Neutrino Mass Experiment [16], which constrain the value of $\sin^2\vartheta_{ee}$ for m_4^2 between about 10 and 3×10^4 eV^2. Figure 14 shows the constraints in the $\sin^2 2\vartheta_{ee} - \Delta m_{41}^2$ plane that we obtained with a χ^2 analysis of the Mainz data in Ref. [16]. From the comparison with the allowed regions obtained from the global fit of ν_e disappearance data shown in Fig. 14 one can see that the Mainz data constrain Δm_{41}^2 to be smaller than about 10^4 eV^2 at about 90% C.L. This is confirmed by the results of the combined fit shown in Fig. 15.

The KATRIN experiment (see Ref. [81]), which will start in 2015 [82], may be able to improve dramatically the upper limits on m_4 and maybe see its effects on the electron spectrum [83].

The heavy neutrino mass m_4 also has an effect in neutrinoless double-β decay (see Refs. [84–87]), if massive neutrinos are Majorana particles (see Refs. [1–3]). Considering Eq. (41), the contribution of the heavy neutrino mass m_4 to the effective Majorana mass

$$m_{\beta\beta} = \left|\sum_k U_{ek}^2 m_k\right| \tag{43}$$

is given by

$$m_{\beta\beta}^{(4)} \simeq |U_{e4}|^2\sqrt{\Delta m_{41}^2}. \tag{44}$$

Figure 16 shows the marginal $\Delta\chi^2 = \chi^2 - \chi^2_{\rm min}$ as a function of $m_{\beta\beta}^{(4)}$ obtained from the global fit. One can see that $m_{\beta\beta}^{(4)}$ is bounded from below and it is likely to be larger than about 10^{-2} eV, a value which may be reached in the next generation of neutrinoless double-β decay experiments (see Refs. [87,88]). Of course, if the three light neutrinos ν_1, ν_2, ν_3 are quasidegenerate at a mass scale larger than about 10^{-2} eV, the contribution of $m_{\beta\beta}^{(4)}$ can cancel with that of the three light neutrinos. Such an unfortunate cancellation can also happen if the masses of the three light neutrinos follow an inverted hierarchy [89,90], since in that case their contribution to the effective Majorana mass is [85]

$$1.4 \times 10^{-2} \lesssim m_{\beta\beta}^{(\rm light)} \lesssim 5.0 \times 10^{-2}\ \text{eV} \quad (\text{IH} - 95\%\text{C.L.}). \tag{45}$$

On the other hand, no cancellation is possible in the case of a normal hierarchy, for which [85]

$$m_{\beta\beta}^{(\rm light)} \lesssim 4.5 \times 10^{-3}\ \text{eV} \qquad (\text{NH} - 95\%\text{C.L.}), \tag{46}$$

and the contribution of $m_{\beta\beta}^{(4)}$ is dominant if it is larger than about 10^{-2} eV. Figure 17 shows the allowed values of $m_{\beta\beta}$ as functions of the lightest neutrino mass in the two 3 + 1 schemes with a normal (left) and inverted (right) mass spectra of the three light neutrinos. We have drawn also the curves, which delimit the three-neutrino mixing allowed regions [85]. One can see that practically the situation is reversed with respect to the three-neutrino mixing case (see also the discussion in Ref. [87]), in which $m_{\beta\beta}$ is predicted to be large in the inverted spectrum and can vanish in the normal spectrum. In the 3 + 1 case $m_{\beta\beta}$

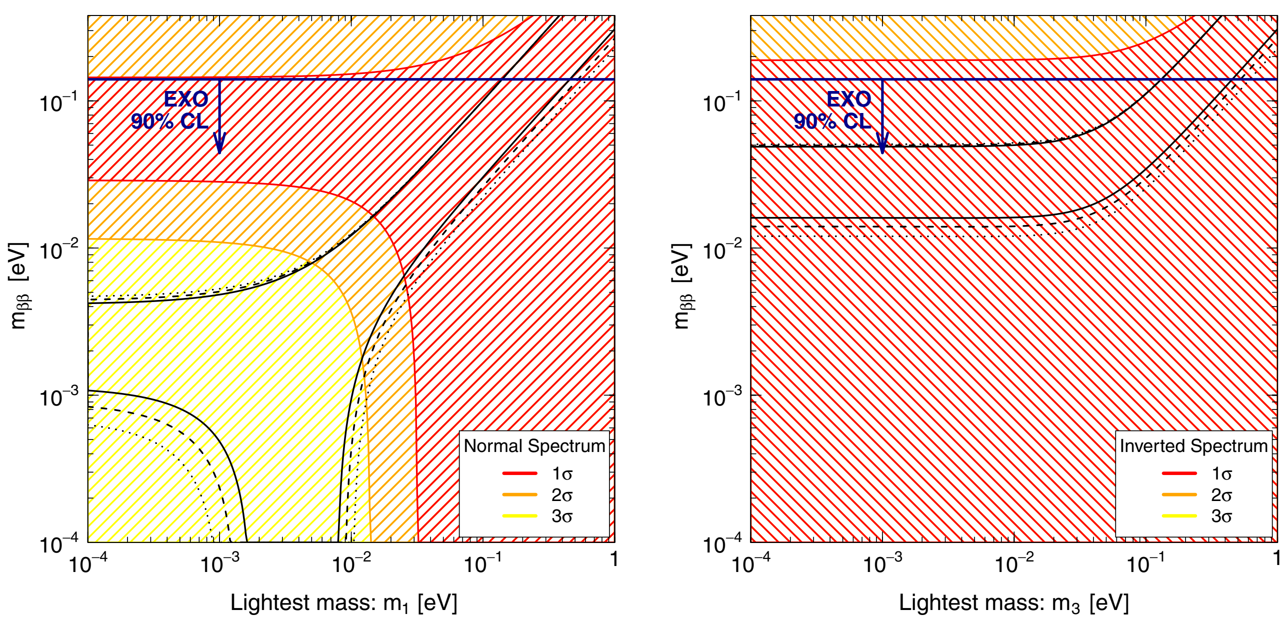

FIG. 17 (color online). Allowed ranges of the effective Majorana mass $|m_{\beta\beta}|$ as a function of the lightest neutrino mass in the two 3 + 1 schemes with a normal (left) and inverted (right) mass spectra of the three light neutrinos ν_1, ν_2, ν_3. The black lines delimit the three-neutrino mixing allowed regions at 1σ (solid lines), 2σ (dashed lines), 3σ (dotted lines) [85].

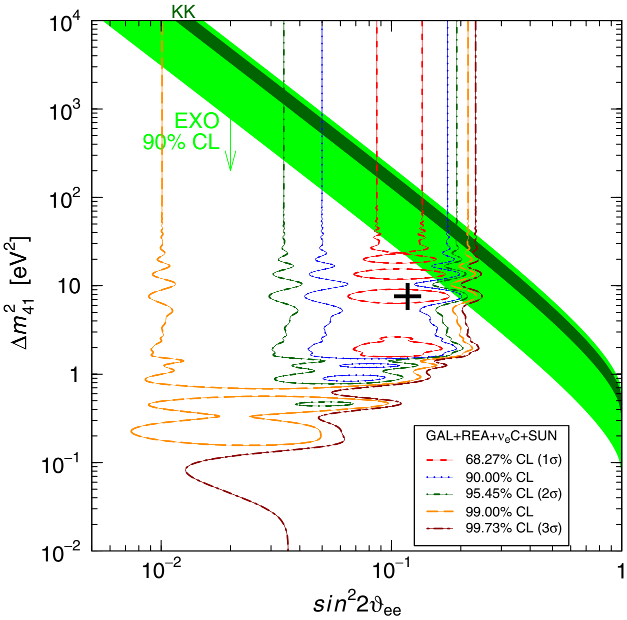

FIG. 18 (color online). Comparison of the allowed regions in the $\sin^2 2\vartheta_{ee} - \Delta m^2_{41}$ plane obtained from the global fit of ν_e disappearance data (same as in Fig. 12) and the bound in the no-cancellation case (47) corresponding to the 90% C.L. upper bound for $m_{\beta\beta}$ obtained in the EXO experiment taking into account nuclear matrix element uncertainties [17] (shaded band). The dark shaded (dark green) band corresponds to the 1σ Klapdor-Kleingrothaus *et al.* range of $m_{\beta\beta}$ [18].

can have any value in the inverted spectrum, whereas in the normal spectrum it is likely to be large if the three light neutrino masses are hierarchical, i.e., if $m_1 \ll m_2 \ll m_3$.

Let us consider the "no-cancellation" case, in which

$$m_{\beta\beta} \geq m^{(4)}_{\beta\beta} \quad \text{(no-cancellation)}. \tag{47}$$

In this case, as shown in Fig. 16, large values of $m^{(4)}_{\beta\beta}$ are excluded by the currently most stringent upper bound for $m_{\beta\beta}$ obtained in the EXO experiment [17] (the vertical shaded band in Fig. 16 is the 90% C.L. EXO bound taking into account nuclear matrix element uncertainties). This limit implies the upper bound on $\Delta m^2_{41} \simeq (m^{(4)}_{\beta\beta}/|U_{e4}|^2)^2$ as a function of $\sin^2 2\vartheta_{ee}$ shown in Fig. 18. One can see that parts of the high-Δm^2_{41} regions allowed by the global fit are disfavored by the EXO bound. However, the large nuclear matrix element uncertainties do not allow one to establish a precise bound. From Fig. 18, one can also see that the putative Klapdor-Kleingrothaus *et al.* 1σ range of $m_{\beta\beta}$ [18] implies a rather large value of Δm^2_{41}, around 100–200 eV^2. In this case, the oscillation length is very short, of the order of 1 cm for neutrinos with energy of the order of 1 MeV, as reactor neutrinos and neutrinos emitted by radioactive sources. Hence, it will be practically impossible to observe a variation of the event rate characteristic of oscillations in future very short-baseline reactor neutrino experiments [91,92] and radioactive source experiments [93–96] (see also Refs. [15,97]).

Finally, considering cosmological measurements one must say that they are a powerful probe of the number of neutrinos and of neutrino masses at the eV scale (see Refs. [15,98,99]), but the analysis requires many assumptions on the cosmological model and its details. A comparison of the results of the fit of short-baseline oscillation data is beyond the scope of this paper. We can only say that the analysis of cosmological data in the framework of the standard ΛCDM [48,100–105] allow the existence of a sterile neutrino thermalized in the early Universe, but restricts its mass to be less than about 1 eV (a possible suppression of the sterile neutrino thermalization with a large lepton asymmetry has been discussed recently in Refs. [106,107]). If this constraint is correct, the upper bound on Δm^2_{41} is about 1 eV^2, which is much more restrictive than those of β decay in Fig. 14 and neutrinoless double-β decay in Fig. 18.

VI. CONCLUSIONS

In this paper, we presented a complete update of the analysis of ν_e and $\bar{\nu}_e$ disappearance experiments in terms of neutrino oscillations in the framework of 3 + 1 neutrino mixing. We have shown that the Gallium anomaly, the reactor anomaly, solar neutrino data, and ν_eC scattering data are compatible with short-baseline oscillations with an amplitude $\sin^2 2\vartheta_{ee}$ between about 0.03 and 0.2 and a squared-mass difference Δm^2_{41} larger than about 0.5 eV^2 at 95% C.L. Assuming the mass hierarchy in Eq. (40), we have shown that the heavy neutrino mass m_4 is observable in β-decay experiments and neutrinoless double-β decay experiments. The very recent Mainz β-decay data [16] constrain Δm^2_{41} to be smaller than about 10^4 eV^2 at 95% C.L. For Majorana neutrinos, the recent EXO limit on the effective Majorana mass in neutrinoless double-β decay [17] give a more stringent constraint, which can vary between about 10^2 and 10^3 eV^2 depending on the nuclear matrix element uncertainties if there are no cancellations between the contribution of ν_4 and that of the three light neutrinos. We think that our results are interesting for the many projects which will search in the next years effects of light sterile neutrinos with electron neutrino and antineutrino radioactive sources (see Refs. [15,108,109]), reactor electron antineutrinos (see Refs. [15,110]), and accelerator electron neutrinos [111–113].

ACKNOWLEDGMENTS

The work of Y. F. L. is supported in part by the National Natural Science Foundation of China under Grant No. 11135009. The work of H. W. L. is supported in part by the National Natural Science Foundation of China under Grant No. 11265006.

[1] C. Giunti and C. W. Kim, *Fundamentals of Neutrino Physics and Astrophysics* (Oxford University Press, Oxford, 2007).
[2] S. Bilenky, *Introduction to the Physics of Massive and Mixed Neutrinos*, Lecture Notes in Physics Vol. 817 (Springer, Berlin, 2010).
[3] Z.-z. Xing and S. Zhou, *Neutrinos in Particle Physics*, Astronomy and Cosmology (Zhejiang University Press, Hangzhou, 2011).
[4] M. Laveder, Nucl. Phys. B, Proc. Suppl. **168**, 344 (2007); *Workshop on Neutrino Oscillation Physics, Otranto, Lecce, Italy, 2006* (NOW, Otranto, 2006).
[5] C. Giunti and M. Laveder, Mod. Phys. Lett. A **22**, 2499 (2007).
[6] C. Giunti and M. Laveder, Phys. Rev. C **83**, 065504 (2011).
[7] T. A. Mueller *et al.*, Phys. Rev. C **83**, 054615 (2011).
[8] P. Huber, Phys. Rev. C **84**, 024617 (2011).
[9] G. Mention, M. Fechner, Th. Lasserre, Th. Mueller, D. Lhuillier, M. Cribier, and A. Letourneau, Phys. Rev. D **83**, 073006 (2011).
[10] A. Aguilar *et al.* (LSND Collaboration), Phys. Rev. D **64**, 112007 (2001).
[11] A. A. Aguilar-Arevalo *et al.* (MiniBooNE Collaboration), arXiv:1207.4809.
[12] C. Giunti, M. Laveder, Y. Li, Q. Liu, and H. Long (to be published).
[13] S. Schael *et al.* (ALEPH, DELPHI, L3, OPAL, SLD, LEP Electroweak Working Group, SLD Electroweak Group, SLD Heavy Flavour Group), Phys. Rep. **427**, 257 (2006).
[14] D. Frekers *et al.*, Phys. Lett. B **706**, 134 (2011).
[15] K. N. Abazajian *et al.*, arXiv:1204.5379.
[16] C. Kraus, A. Singer, K. Valerius, and C. Weinheimer, arXiv:1210.4194.
[17] M. Auger *et al.* (EXO Collaboration), Phys. Rev. Lett. **109**, 032505 (2012).
[18] H. V. Klapdor-Kleingrothaus and I. V. Krivosheina, Mod. Phys. Lett. A **21**, 1547 (2006).
[19] S. M. Bilenky, C. Giunti, and W. Grimus, Prog. Part. Nucl. Phys. **43**, 1 (1999).
[20] M. Maltoni, T. Schwetz, M. Tortola, and J. Valle, New J. Phys. **6**, 122 (2004).
[21] A. Strumia and F. Vissani, arXiv:hep-ph/0606054.
[22] M. C. Gonzalez-Garcia and M. Maltoni, Phys. Rep. **460**, 1 (2008).
[23] C. Giunti and Y. Li, Phys. Rev. D **80**, 113007 (2009).
[24] A. Palazzo, Phys. Rev. D **83**, 113013 (2011).
[25] A. Palazzo, Phys. Rev. D **85**, 077301 (2012).
[26] A. Palazzo, *Neutrino Oscillation Workshop, 9–16 September 2012, Conca Specchiulla, Otranto, Italy* (NOW, Otranto, 2012).
[27] J. Conrad and M. Shaevitz, Phys. Rev. D **85**, 013017 (2012).
[28] C. Giunti and M. Laveder, Phys. Lett. B **706**, 200 (2011).
[29] M. Galeazzi, F. Fontanelli, F. Gatti, and S. Vitale, Phys. Rev. Lett. **86**, 1978 (2001).
[30] P. Anselmann *et al.* (GALLEX), Phys. Lett. B **342**, 440 (1995).
[31] W. Hampel *et al.* (GALLEX), Phys. Lett. B **420**, 114 (1998).
[32] F. Kaether, W. Hampel, G. Heusser, J. Kiko, and T. Kirsten, Phys. Lett. B **685**, 47 (2010).
[33] J. N. Abdurashitov *et al.* (SAGE Collaboration), Phys. Rev. Lett. **77**, 4708 (1996).
[34] J. N. Abdurashitov *et al.* (SAGE Collaboration), Phys. Rev. C **59**, 2246 (1999).
[35] J. N. Abdurashitov *et al.* (SAGE Collaboration), Phys. Rev. C **73**, 045805 (2006).
[36] J. N. Abdurashitov *et al.* (SAGE Collaboration), Phys. Rev. C **80**, 015807 (2009).
[37] J. N. Bahcall, Phys. Rev. C **56**, 3391 (1997).
[38] D. Krofcheck *et al.*, Phys. Rev. Lett. **55**, 1051 (1985).
[39] D. Krofcheck, Ph.D. thesis, The Ohio State University, 1987.
[40] W. C. Haxton, Phys. Lett. B **431**, 110 (1998).
[41] J. N. Bahcall, *Neutrino Astrophysics* (Cambridge University Press, Cambridge, England, 1989).
[42] J. Beringer *et al.* (Particle Data Group), Phys. Rev. D **86**, 010001 (2012).
[43] W. Hampel and L. Remsberg, Phys. Rev. C **31**, 666 (1985).
[44] National Nuclear Data Center, Brookhaven National Laboratory, http://www.nndc.bnl.gov/logft/.
[45] C. Giunti and M. Laveder, Phys. Rev. D **82**, 113009 (2010).
[46] C. Giunti and M. Laveder, Phys. Rev. D **84**, 073008 (2011).
[47] C. Giunti and M. Laveder, Phys. Rev. D **84**, 093006 (2011).
[48] M. Archidiacono, N. Fornengo, C. Giunti, and A. Melchiorri, Phys. Rev. D **86**, 065028 (2012).
[49] Bugey, B. Achkar *et al.*, Nucl. Phys. **B434**, 503 (1995).
[50] Bugey, Y. Declais *et al.*, Phys. Lett. B **338**, 383 (1994).
[51] A. Kuvshinnikov, L. Mikaelyan, S. Nikolaev, M. Skorokhvatov, and A. Etenko, JETP Lett. **54**, 253 (1991).
[52] G. Zacek *et al.* (CalTech-SIN-TUM Collaboration), Phys. Rev. D **34**, 2621 (1986).
[53] A. Hoummada, S. L. Mikou, G. Bagieu, J. Cavaignac, and D. H. Koang, Appl. Radiat. Isot. **46**, 449 (1995).
[54] Krasnoyarsk, G. S. Vidyakin *et al.*, Sov. Phys. JETP **71**, 424 (1990).
[55] M. Maltoni and T. Schwetz, Phys. Rev. D **68**, 033020 (2003).
[56] B. T. Cleveland *et al.* (Homestake Collaboration), Astrophys. J. **496**, 505 (1998).
[57] J. N. Abdurashitov *et al.* (SAGE Collaboration), J. Exp. Theor. Phys. **95**, 181 (2002).
[58] J. Hosaka *et al.* (Super-Kamkiokande Collaboration), Phys. Rev. D **73**, 112001 (2006).
[59] J. Cravens *et al.* (Super-Kamkiokande Collaboration), Phys. Rev. D **78**, 032002 (2008).
[60] K. Abe *et al.* (Super-Kamkiokande Collaboration), Phys. Rev. D **83**, 052010 (2011).
[61] M. Smy (Super-Kamkiokande Collaboration), in *XXV International Conference on Neutrino Physics and Astrophysics, 2012* (Neutrino, Kyoto, 2012).
[62] Q. R. Ahmad *et al.* (SNO Collaboration), Phys. Rev. Lett. **89**, 011302 (2002).
[63] B. Aharmim *et al.* (SNO Collaboration), Phys. Rev. C **72**, 055502 (2005).
[64] B. Aharmim *et al.* (SNO Collaboration), Phys. Rev. Lett. **101**, 111301 (2008).
[65] G. Bellini *et al.* (Borexino Collaboration), Phys. Rev. Lett. **107**, 141302 (2011).

[66] G. Bellini *et al.* (Borexino Collaboration), Phys. Rev. Lett. **108**, 051302 (2012).
[67] A. Gando *et al.* (KamLAND Collaboration), Phys. Rev. D **83**, 052002 (2011).
[68] D. Dooling, C. Giunti, K. Kang, and C. W. Kim, Phys. Rev. D **61**, 073011 (2000).
[69] C. Giunti, M. C. Gonzalez-Garcia, and C. Pena-Garay, Phys. Rev. D **62**, 013005 (2000).
[70] F. P. An *et al.* (Daya Bay Collaboration), Phys. Rev. Lett. **108**, 171803 (2012).
[71] S.-B. Kim *et al.* (RENO Collaboration), Phys. Rev. Lett. **108**, 191802 (2012).
[72] S. M. Bilenky, C. Giunti, and W. Grimus, Eur. Phys. J. C **1**, 247 (1998).
[73] A. de Gouvea and T. Wytock, Phys. Rev. D **79**, 073005 (2009).
[74] C. Giunti and M. Laveder, Phys. Rev. D **85**, 031301 (2012).
[75] B. Aharmim *et al.* (SNO Collaboration), Phys. Rev. C **81**, 055504 (2010).
[76] B. Aharmim *et al.* (SNO Collaboration), arXiv:1109.0763.
[77] J. N. Bahcall and M. H. Pinsonneault, Phys. Rev. Lett. **92**, 121301 (2004).
[78] B. E. Bodmann *et al.* (KARMEN Collaboration), Phys. Lett. B **332**, 251 (1994).
[79] B. Armbruster *et al.*, Phys. Rev. C **57**, 3414 (1998).
[80] L. B. Auerbach *et al.* (LSND Collaboration), Phys. Rev. C **64**, 065501 (2001).
[81] E. Otten and C. Weinheimer, Rep. Prog. Phys. **71**, 086201 (2008).
[82] J. Wolf (KATRIN Collaboration), in *International Symposium on Neutrino Physics and Beyond, 2012* (NPB, Shenzhen, 2012).
[83] A. Esmaili and O. L. G. Peres, Phys. Rev. D **85**, 117301 (2012).
[84] J. Gomez-Cadenas, J. Martin-Albo, M. Mezzetto, F. Monrabal, and M. Sorel, Riv. Nuovo Cimento **35**, 29 (2012).
[85] S. M. Bilenky and C. Giunti, Mod. Phys. Lett. A **27**, 1230015 (2012).
[86] J. D. Vergados, H. Ejiri, and F. Simkovic, Rep. Prog. Phys. **75**, 106301 (2012).
[87] W. Rodejohann, J. Phys. G **39**, 124008 (2012).
[88] O. Cremonesi, in *Neutrino Oscillation Workshop, Conca Specchiulla, Otranto, Italy, 2012* (NOW, Otranto, 2012).
[89] J. Barry, W. Rodejohann, and H. Zhang, J. High Energy Phys. 07 (2011) 091.
[90] Y. Li and S. Liu, Phys. Lett. B **706**, 406 (2012).
[91] A. P. Serebrov *et al.*, arXiv:1205.2955.
[92] A. V. Derbin, A. S. Kayunov, and V. N. Muratova, arXiv:1204.2449.
[93] A. Ianni, D. Montanino, and G. Scioscia, Eur. Phys. J. C **8**, 609 (1999).
[94] V. N. Gavrin, V. V. Gorbachev, E. P. Veretenkin, and B. T. Cleveland, arXiv:1006.2103.
[95] M. Cribier, M. Fechner, T. Lasserre, A. Letourneau, D. Lhuillier, G. Mention, D. Franco, V. Kornoukhov, and S. Schönert, Phys. Rev. Lett. **107**, 201801 (2011).
[96] A. Bungau *et al.*, arXiv:1205.4419.
[97] T. Lasserre, in *Neutrino 2012 Conference, Kyoto, Japan, 2012* (2012).
[98] Y. Y. Y. Wong, Annu. Rev. Nucl. Part. Sci. **61**, 69 (2011).
[99] G. Steigman, arXiv:1208.0032.
[100] B. A. Reid, L. Verde, R. Jimenez, and O. Mena, J. Cosmol. Astropart. Phys. 01 (2010) 003.
[101] M. C. Gonzalez-Garcia, M. Maltoni, and J. Salvado, J. High Energy Phys. 08 (2010) 117.
[102] J. Hamann, S. Hannestad, G. G. Raffelt, I. Tamborra, and Y. Y. Wong, Phys. Rev. Lett. **105**, 181301 (2010).
[103] J. Hamann, S. Hannestad, G. G. Raffelt, and Y. Y. Wong, J. Cosmol. Astropart. Phys. 09 (2011) 034.
[104] M. Archidiacono, E. Calabrese, and A. Melchiorri, Phys. Rev. D **84**, 123008 (2011).
[105] S. Joudaki, K. N. Abazajian, and M. Kaplinghat, arXiv:1208.4354.
[106] S. Hannestad, I. Tamborra, and T. Tram, J. Cosmol. Astropart. Phys. 07 (2012) 025.
[107] A. Mirizzi, N. Saviano, G. Miele, and P. D. Serpico, Phys. Rev. D **86**, 053009 (2012).
[108] A. Ianni, in *Neutrino Oscillation Workshop, Conca Specchiulla, Otranto, Italy, 2012* (NOW, Otranto, 2012).
[109] J. Link, in *Neutrino Oscillation Workshop, Conca Specchiulla, Otranto, Italy, 2012* (NOW, Otranto, 2012).
[110] J. Gaffiot, in *Neutrino Oscillation Workshop, Conca Specchiulla, Otranto, Italy, 2012* (NOW, Otranto, 2012).
[111] M. Antonello *et al.*, arXiv:1203.3432.
[112] L. Stanco, in *Neutrino Oscillation Workshop, Conca Specchiulla, Otranto, Italy, 2012* (NOW, Otranto, 2012).
[113] D. Gibin, in *Neutrino Oscillation Workshop, Conca Specchiulla, Otranto, Italy, 2012* (NOW, Otranto, 2012).